



# Novel Mechanism for Surface Layer Shedding and Regenerating in Bacteria Exposed to Metal-Contaminated Conditions

Archjana Chandramohan<sup>1</sup>, Elodie Duprat<sup>2</sup>, Laurent Remusat<sup>2</sup>, Severine Zirah<sup>1</sup>, Carine Lombard<sup>1</sup> and Adrienne Kish<sup>1\*</sup>

<sup>1</sup> Unité Molécules de Communication et Adaptation des Microorganismes (MCAM), Muséum National d'Histoire Naturelle, CNRS UMR 7245, Paris, France, <sup>2</sup> Institut de Minéralogie, Physique des Matériaux et de Cosmochimie (IMPMC), Sorbonne Université, Muséum National d'Histoire Naturelle, CNRS UMR 7590, IRD UMR 206, Paris, France

## OPEN ACCESS

### Edited by:

Stéphane Pesce,  
National Research Institute of Science  
and Technology for Environment  
and Agriculture (IRSTEA), France

### Reviewed by:

Mariusz Cycoń,  
Medical University of Silesia, Poland  
Sukhendu Mandal,  
University of Calcutta, India

### \*Correspondence:

Adrienne Kish  
adrienne.kish@mnhn.fr

### Specialty section:

This article was submitted to  
Microbiotechnology, Ecotoxicology  
and Bioremediation,  
a section of the journal  
Frontiers in Microbiology

**Received:** 13 September 2018

**Accepted:** 11 December 2018

**Published:** 15 January 2019

### Citation:

Chandramohan A, Duprat E,  
Remusat L, Zirah S, Lombard C and  
Kish A (2019) Novel Mechanism  
for Surface Layer Shedding  
and Regenerating in Bacteria  
Exposed to Metal-Contaminated  
Conditions. *Front. Microbiol.* 9:3210.  
doi: 10.3389/fmicb.2018.03210

Surface layers (S-layers) are components of the cell walls throughout the Bacteria and the Archaea that provide protection for microorganisms against diverse environmental stresses, including metal stress. We have previously characterized the process by which S-layers serve as a nucleation site for metal mineralization in an archaeon for which the S-layer represents the only cell wall component. Here, we test the hypothesis originally proposed in cyanobacteria that a “shedding” mechanism exists for replacing S-layers that have become mineral-encrusted, using *Lysinibacillus* sp. TchlII 20n38, metallotolerant gram-positive bacterium, as a model organism. We characterize for the first time a mechanism for resistance to metals through S-layer shedding and regeneration. S-layers nucleate the formation of Fe-mineral on the cell surface, depending on physiological state of the cells and metal exposure times, leading to the encrustation of the S-layer and changes in the cell morphology as observed by scanning electron microscopy. Using Nanoscale Secondary Ion Mass Spectrometry, we show that mineral-encrusted S-layers are shed by the bacterial cells after a period of latency (2 days under the conditions tested) in a heterogeneous fashion likely reflecting natural variations in metal stress resistance. The emerging cells regenerate new S-layers as part of their cell wall structure. Given the wide diversity of S-layer bearing prokaryotes, S-layer shedding may represent an important mechanism for microbial survival in metal-contaminated environments.

**Keywords:** S-layer, metal, biomineralization, metallotolerance, *Lysinibacillus*

## INTRODUCTION

Environmental contamination by metals and radionuclides from activities such as mining and nuclear power generation pose a serious risk to human health. The sudden, accidental release of high concentrations of iron from acid mine drainage from the Gold King Mine polluted the Animas River in 2015, mixing downstream with phosphates from agricultural runoff (Rodriguez-Freire et al., 2016). Metal contamination affected both water supplies from soluble metals, and sediments after the sedimentation of the majority of released metals. Sampling of soils contaminated by metals

and radionuclides near the former Chernobyl nuclear reactor site (Chapon et al., 2012) and in uranium mining waste piles in Germany (Pollmann et al., 2006) have identified bacteria of the genus *Lysinibacillus* tolerant to these contaminants. *Lysinibacillus* [formerly classified as part of the *Bacillus* genus (Ahmed et al., 2007)] gram-positive bacteria, with a peptidoglycan cell wall enclosed by a surface layer (“S-layer”) attached non-covalently to the lipopolysaccharides of the outer membrane (reviewed in Sleytr et al., 2014). These S-layers have proven to be a key mechanism for metal tolerance in *Lysinibacillus* as they have been shown to bind U, Pd(II), Cu, Pt(II), and Au(III) (Pollmann et al., 2006).

S-Layers, however are not unique to *Lysinibacillus*. They are common components of the cell envelopes of both bacteria and archaea. S-layers are formed by self-assembly of repeated protein monomers into ordered structures (oblique, square, or hexagonal) depending on the number of subunits composing the ordered structure. This self-assembly occurs even in the absence of cells *in vitro*; a capacity has been exploited in biotechnology in everything from the development of vaccine to nanomaterials to filtration technologies (Sleytr et al., 2011).

S-Layers form the interaction interface between prokaryotic cells and their external environment, and are therefore in contact with metals and other ions present. Nucleation of mineralization by S-layers was first noted in cyanobacteria by Schultze-Lam et al. (1992). Cyanobacterial S-layers were demonstrated to nucleate the formation of carbonates of calcium, magnesium, and strontium (Schultze-Lam and Beveridge, 1994). Schultze-Lam et al. (1992) proposed the hypothesis that mineral-encrusted S-layers are shed from cyanobacteria as part of a protective mechanism to ensure that essential cell activities are maintained despite cell wall mineralization. This hypothesis was, however, never fully tested. Since then, S-layer nucleation of mineralization has been observed in a range of bacteria (Konhauser et al., 1994; Phoenix et al., 2000) and archaea (Kish et al., 2016).

Here, we describe the shedding and regeneration of mineral-encrusted S-layers in the metallotolerant environmental isolate *Lysinibacillus* sp. TchIII 20n38.

## MATERIALS AND METHODS

### Culture and Growth Conditions

The bacterial strain used was an environmental strain isolated in 2009 from soils near a radionuclide-contaminated site (Chapon et al., 2012). This strain, referenced as *Lysinibacillus* sp. TchIII 20n38, was cultured at 30°C in Luria Bertani (LB) medium under aerobic conditions with agitation (180 rpm) to mid-exponential, late-exponential, and stationary growth phases ( $OD_{600\text{ nm}} = 0.3, 0.6, \text{ and } 1.0$ , respectively). The culture medium was then removed and the cells washed in MilliQ-H<sub>2</sub>O by gentle centrifugation ( $2600 \times g$ , 15 min, room temperature). In order to determine the mechanisms of resistance of *Lysinibacillus* sp. TchIII 20n38 cells to the presence of heavy metals, the cells were resuspended to an equivalent cell density in a Fe-rich solution at a similar pH to that found in the Chernobyl isolation (10 mM NaH<sub>2</sub>PO<sub>4</sub>, 10 mM FeSO<sub>4</sub>, pH = 4.5), and agitated (150 rpm, 30°C) with

for up to 5 days. Cells were filtered and observed by scanning electron microscopy (SEM) as described below.

### Mineralization Recovery Time Course

In order to test the hypothesis that mineral-encrusted S-layers are shed and regenerated, a time course of recovery was followed after Fe-mineralization as follows: *Lysinibacillus* sp. TchIII 20n38 cells were grown to mid-exponential growth phase ( $OD_{600\text{ nm}} = 0.3$ ) in LB (30°C, 180 rpm). The culture medium was then removed and the cells washed in MilliQ-H<sub>2</sub>O by gentle centrifugation ( $2600 \times g$ , 15 min, room temperature). The cells were then resuspended to an equivalent cell density in either a mineralization solution (10 mM NaH<sub>2</sub>PO<sub>4</sub>, 10 mM FeSO<sub>4</sub>, pH = 4.5), or a nutrient-free buffered solution at the same pH (10 mM NaH<sub>2</sub>PO<sub>4</sub>, pH = 4.5), and agitated (30°C, 150 rpm) for 16 h. The mineralization solution was then removed and the cells washed in MilliQ-H<sub>2</sub>O by gentle centrifugation ( $2600 \times g$ , 15 min, room temperature), and replaced by growth medium (LB, or labeled growth medium).

For nanoscale secondary ion mass spectrometry (NanoSIMS) experiments, LB was replaced with a defined growth medium approximating LB but containing either <sup>14</sup>N or <sup>15</sup>N (Celtone®, Cambridge Isotopes, United States). While specified for use with bacteria for isotope analyses, this media was found to contain inhibitory concentrations of trace metals, which we were able to remove by precipitation by addition of an excess of buffered phosphate (10 mM) over 24 h with agitation at 150 rpm, followed by filtration using a 0.22 μm filter. This metal-depleted medium containing 5 g/L Celtone® was completed with 5 g/L acetate as a C-source, and basal salts (15 mM ammonium sulfate, 0.2 mM MgSO<sub>4</sub>, 17.6 mM KH<sub>2</sub>PO<sub>4</sub>, 32.7 mM NaH<sub>2</sub>PO<sub>4</sub>), as determined by our preliminary optimized experiments with *Lysinibacillus* sp. TchIII 20n38. In addition, cultures grown in the presence of <sup>14</sup>N rather than <sup>15</sup>N rapidly ceased vegetative growth and sporulated. Therefore instead of a standard labeling medium composed of both <sup>14</sup>N and <sup>15</sup>N, a 100% <sup>15</sup>N-labeled medium, was used to follow the time course of recovery after Fe-exposure. An additional culture was resuspended in a 100% <sup>14</sup>N medium and immediately sampled as a baseline control for N isotope abundances. Cultures were incubated in the <sup>15</sup>N-labeled medium at 30°C with agitation (180 rpm) over a time course of recovery, for both mineralized (M) and non-mineralized (NM) cultures. Aliquots were removed immediately after addition of growth medium (T0), and then every 24 h (1, 2 days). At each time point, approximately 20 mL aliquots were removed for optical density measurements, optical microscopy verification of cell morphology, and filtered for SEM observations and NanoSIMS analyses as described below. Abiotic (non-inoculated) controls were used for comparison to distinguish mineralization due to the presence of *Lysinibacillus* sp. TchIII 20n38 cells.

### Scanning Electron Microscopy

Aliquots of bacterial cultures as well as abiotic controls (not inoculated with *Lysinibacillus* sp. TchIII 20n38 cells) were filtered through a 0.2 μm GTTP isopore polycarbonate filters using a Swinnex filter holder (Merck Millipore, Darmstadt, Germany). Filters were then air-dried, mounted on aluminum supports

with carbon tape, and coated with carbon (7–8 nm thickness), gold (7 nm thickness), or platinum (5 nm thickness). SEM observations were performed using two different instruments; a Hitachi SU 3500 SEM installed at the electron microscopy platform of the Muséum National d'Histoire Naturelle (Paris, France), and a Zeiss Ultra 55 field emission gun SEM equipped with a Bruker EDS QUANTAX detector (Bruker Corporation, Houston, TX, United States) installed at IMPMC (Sorbonne Université, Paris, France). For observations using the Hitachi SU 3500 instrument observations were made in secondary electron mode with an acceleration voltage of 15 kV. SEM-FEG images were acquired in secondary electron mode using with the Zeiss Ultra 55 instrument with an in column detector (InLens) at 2 to 5 kV and a working distance of 3 mm. Energy dispersive X-ray spectroscopy (EDX) analyses were performed at 15 kV and a working distance of 7.5 mm after calibration with reference copper.

## Nano Secondary Ion Mass Spectrometry

Nano secondary ion mass spectrometry sample preparations followed the protocol of Miot et al. (2015). Briefly, aliquots of bacterial cultures sampled from labeled and unlabeled media filtered through 0.2  $\mu\text{m}$  GTTP isopore polycarbonate filters previously Au-coated (20 nm thickness) using a Swinnex filter holder (Merck Millipore, Darmstadt, Germany). Quantitative ion images were recorded by the NanoSIMS50 (Cameca, Gennevilliers, France) installed at the National Museum of Natural History of Paris, France. All measurements were performed using the same analytical conditions. A Cs + primary beam of 0.8 pA scanned an area of 20  $\mu\text{m}$   $\times$  20  $\mu\text{m}$ , divided into 256 pixels  $\times$  256 pixels, with a counting time of 1 ms per pixel. Secondary ion images of  $^{31}\text{P}^{16}\text{O}^-$ ,  $^{12}\text{C}^{14}\text{N}^-$ , and  $^{12}\text{C}^{15}\text{N}^-$  were recorded. The mass resolution power was adjusted to 9000 to resolve isobaric interferences at mass 27 such as  $^{13}\text{C}^{14}\text{N}^-$  or  $^{11}\text{B}^{16}\text{O}$  from  $^{12}\text{C}^{15}\text{N}^-$ . Before any analysis, the surface of each sample was pre-sputtered during 5 min with a 80 pA Cs- primary ion beam over 30  $\mu\text{m}$   $\times$  30  $\mu\text{m}$  to eliminate the contamination of the surface, and reached the stable state of sputtering (Thomen et al., 2014). Instrument stability was verified throughout the session using a type 3 kerogen standard. NanoSIMS data were then processed using the IMAGE software (L. Nittler, Carnegie Institution for Science, Washington, DC, United States).

## Statistical Analyses

The preference of this strain of *Lysinibacillus* for  $^{15}\text{N}$  to maintain vegetative growth eliminated the possibility of using a  $^{14}\text{N}$  control throughout the time course of recovery. In order to automatically remove the random noise from all the  $^{12}\text{C}^{14}\text{N}^-$  and  $^{12}\text{C}^{15}\text{N}^-$  NanoSIMS images, we defined  $^{12}\text{C}^{14}\text{N}^-$  and  $^{12}\text{C}^{15}\text{N}^-$  independent thresholds based on their respective distribution for the images of samples that were resuspended in the  $^{14}\text{N}$ -labeled medium. Each elemental distribution was fitted by two Gaussian components (R-package mixtools, Benaglia et al., 2009). We define threshold as the mean of the 97.5th percentile of the first Gaussian component (noise) and the 2.5th percentile of the second one (signal).

For each image, the denoised dataset further used for statistical analyses is composed only of pixels with both  $^{12}\text{C}^{14}\text{N}^-$  and  $^{12}\text{C}^{15}\text{N}^-$  values above the respective thresholds. The isotope abundance  $^{12}\text{C}^{15}\text{N}^- / (^{12}\text{C}^{14}\text{N}^- + ^{12}\text{C}^{15}\text{N}^-)$  of this dataset (hereafter named processed  $^{15}\text{N} / (^{14}\text{N} + ^{15}\text{N})$  ratio) was used to follow the kinetics of incorporation of N (as part of protein production) by non-mineralized and mineralized bacteria. For each image, the distribution of processed  $^{15}\text{N} / (^{14}\text{N} + ^{15}\text{N})$  ratio was fitted using Gaussian mixture modeling (R-package mclust, Scrucca et al., 2016) in order to infer subpopulations of pixels. The best univariate model, composed of  $k$  Gaussian components with either equal or unequal variance, was selected based on Bayesian Information Criterion. The mixing proportions for the components represent the proportions of the  $k$  subpopulations of pixels.

Cluster analysis was performed in order to group the samples according to their subpopulation composition. Each image was described by a vector of 10 values, each corresponding to the sum of the mixing proportions for the Gaussian components whose mean falls in a given  $^{15}\text{N} / (^{14}\text{N} + ^{15}\text{N})$  ratio interval (10 intervals of size 0.1 each). An image-to-image distance matrix generated by computing Bray-Curtis dissimilarity index between all the pairs of vectors was used for hierarchical agglomerative clustering of images (unweighted pair group method with arithmetic mean linkage).

All analyses were conducted in R version 3.2.3 (R Core Team, 2015).

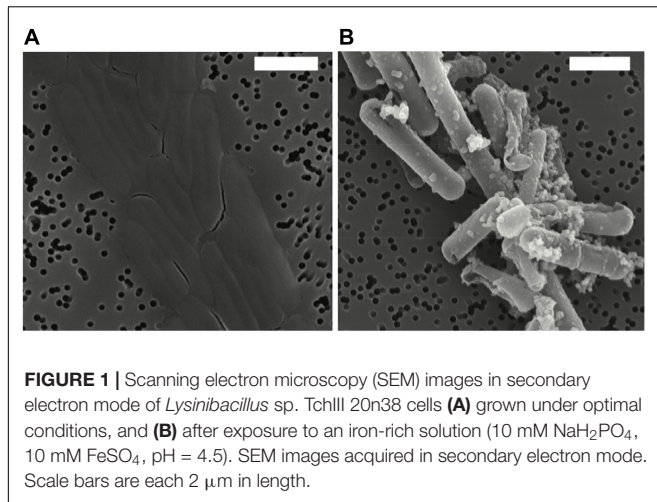
## RESULTS

### *Lysinibacillus* sp. S-Layers Become Encrusted After Exposure to Iron

*Lysinibacillus* sp. TchIII 20n38 was isolated from soils contaminated by radionuclides and metals, resulting in a moderately acidic pH (5.5) (Chapon et al., 2012). Our work with this strain, like other isolates from the same site, has shown that it is resistant to a range of heavy metals and radionuclides (data not shown). To determine the mechanisms of this metal tolerance, we exposed cells to a Fe-rich solution at acidic pH in the absence of the preferred carbon source for this strain, acetate, while maintaining high levels of phosphate required by *Lysinibacillus* sp. Non-metabolic metal-tolerance mechanisms are favored under these conditions.

After exposure, Fe-minerals were observed to form on the surface of *Lysinibacillus* sp. cells leading to complete encrustation of the cells over time (see **Figure 1**). EDX analyses of mineral-encrusted cells confirmed the composition as a Fe-phosphate (see **Supplementary Figure S1**). Some abiotically formed Fe-phosphates were also observed, which were easily distinguishable from mineralized S-layers as aggregates of larger spherically-shaped minerals not associated with cells, and matching the types of minerals observed in non-inoculated controls.

Cells were fully mineral encrusted after 16 h of exposure to the Fe-rich solution, whether cells were exposed in mid-exponential, late-exponential, or stationary growth phase ( $\text{OD}_{600\text{ nm}} = 0.3, 0.6,$



and 1.0, respectively). Longer exposures (20 and 41 h) did not alter the extent mineralization.

Attempts to confirm whether the mineralization observed on *Lysinibacillus* sp. TchIII 20n38 cells was due to a completely non-metabolic process, or whether active metabolism by living cells was necessary for S-layer mineralization were limited due to an inability to obtain dead cells without damaging the S-layer containing cell envelope. This despite multiple trials employing various antibiotics targeting non-cell envelope structures, and testing them over a large range of concentrations and durations [tetracycline (10–2000 μg/mL for 1 h–5 days in LB, buffer, or MilliQ-H<sub>2</sub>O) ofloxacin (10–500 μg/mL), and heat treatments (up to 55°C)]. The fact that *Lysinibacillus* sp. TchIII 20n38 cells grow optimally as heterotrophs without added metals suggests that the role of any metabolic processes in S-layer mineralization was secondary to non-metabolic processes.

## Response to Metal Exposure Depends on Physiological State, Times of Mineralization and Recovery

Replacement of mineral-encrusted cells into a rich growth medium demonstrated that *Lysinibacillus* sp. TchIII 20n38 cells were able to resume proper cell division after complete Fe-mineral encrustation. The exposure of mid-exponential growth phase cells (OD<sub>600 nm</sub> = 0.3) to the Fe-rich solution for 16 h followed by recovery of the cultures in LB showed that cells resumed normal cell division (see **Supplementary Figure S2**). However, the physiological state of the cells during metal encrustation, resulting in various inhibitions of normal vegetative cell growth and division. For mid-exponential growth phase cells, exposures longer than 16 h to the Fe-rich solution resulted in the death of mineralized cells, and the formation of filaments by the small minority of cells observed without mineral-encrustation. In the case of both late-exponential growth phase and stationary phase cultures, even 16 h-long exposures to Fe resulted in sporulation and/or cell death.

## Mineral-Encrusted S-Layers Can Be Shed

Scanning electron microscopy observations were made of mid-exponential growth phase *Lysinibacillus* sp. TchIII 20n38 cells after a 16 h exposure to the Fe-rich solution. Mineralized S-layers devoid of a cell were observed, often with the cells located beside these empty mineralized S-layer shell (see **Figure 2A**, left and right images). After incubation in LB for up to 5 days following Fe-mineralization, cells were seen exiting mineralized S-layer cells, with cell division septa visible (see **Figure 2B**, top and bottom images), in concordance with increases in the optical density of the cultures (see **Supplementary Figure S2**).

## *Lysinibacillus* sp. Cell Morphology Changes During S-Layer Shedding

The cell morphology in both mineralized and non-mineralized cultures was altered over the time course of recovery (see **Figure 3**). In non-mineralized cultures which were kept at the same pH as the mineralized cultures but in the absence of iron, cells gradually shrank in size and became ovoid in shape over 2 days of incubation in the metal-depleted Celtone® medium. While cell death was minimal for non-mineralized cells, dead cells were easily distinguishable due to both their high<sup>12</sup>C<sup>14</sup>N<sup>-</sup> counts due to lack of <sup>15</sup>N incorporation, and their sustained rod shape (see image of non-mineralized cells 1 day in **Figure 4**). Non-mineralized cells also formed intracellular polyphosphate granules between 1 and 2 days of incubation, as evidenced by analyses of <sup>31</sup>P<sup>16</sup>O<sup>-</sup> counts (see **Figure 4**).

Mineralized cultures showed little change over the first day of incubation. On the second day, however, cells were observed outside of their mineralized S-layer shells, with biofilm formation evidenced as a mucoid phenotype (see **Figure 3**) together with increases in optical density of the cultures (see **Supplementary Figure S3**). SDS-PAGE and mass spectrometry confirmed the presence of S-layer glycoproteins throughout the time course of recovery (see **Supplementary Figures S4, S5**, and **Supplementary Tables S1–S4**). Shed, mineralized S-layers maintained the elongated rod shape of non-stressed *Lysinibacillus* sp. TchIII 20n38 cells and restricted <sup>31</sup>P<sup>16</sup>O<sup>-</sup> to their surfaces (see **Figure 4**), likely within the Fe-phosphate minerals analyzed by EDX in **Figure 2**. In comparison, newly emerged cells lacked surface phosphates, some cells concentrating phosphate as intracellular granules (see **Figure 4**). On the third day of incubation, cells in both mineralized and non-mineralized cultures began to sporulate.

## Sub-Populations of Cells Co-exist During Time Course of Recovery

In order to describe the process of S-layer regeneration after mineral encrustation, and to determine if the S-layers were indeed regenerated, we followed the recovery of *Lysinibacillus* sp. TchIII 20n38 cells over time after Fe-mineral encrustation. Both SEM observations of cell morphology and NanoSIMS analyses of cell activity using incorporation of nitrogen, needed for the production of new S-layer proteins. <sup>15</sup>N-incorporation

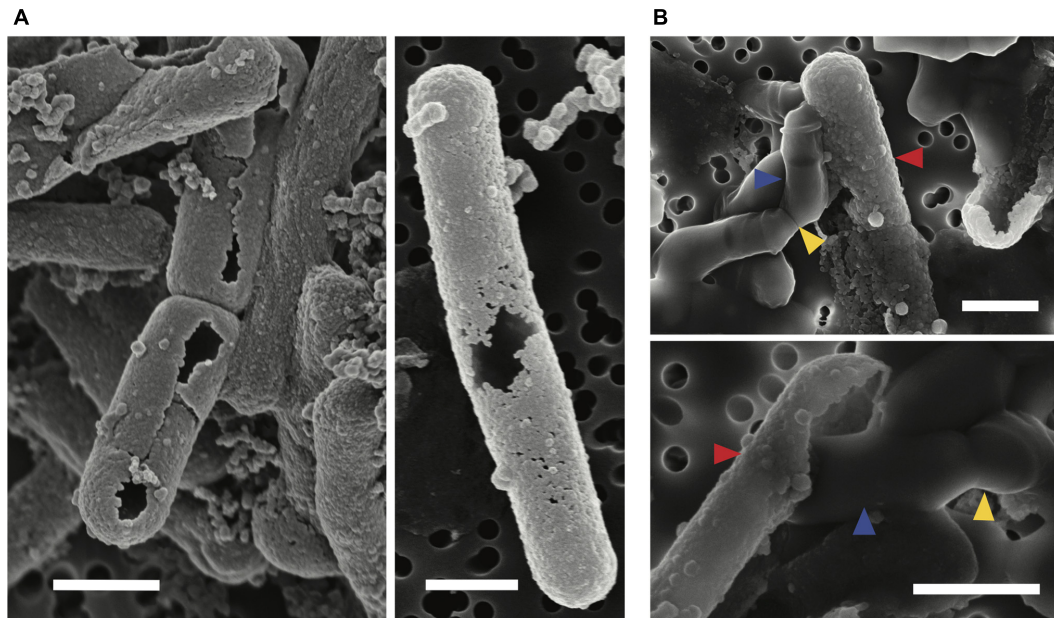


**FIGURE 2** | S-layer mineralization after exposure to Fe as observed by SEM in secondary electron mode. **(A)** Empty mineralized S-layer “shell” lacking a cell observed by SEM (secondary electron mode) after a 16 h exposure of a mid-exponential growth phase culture of *Lysinibacillus* sp. TchlII 20n38 to the Fe-rich solution. Empty S-layer mineral encrustation can be thick (left-side image) or thinner and “lacy” (right-side image). **(B)** Top and bottom images show cells emerging from shed mineralized S-layers. Cells were in mid-exponential growth phase prior to exposure to Fe, followed by incubated in LB for up to 5 days (37°C, 180 rpm). Blue arrows show emerging cells. Red arrows indicate mineralized S-layers. Yellow arrows indicate cell division septa. Scale bars for all images are 1  $\mu\text{m}$  in length.

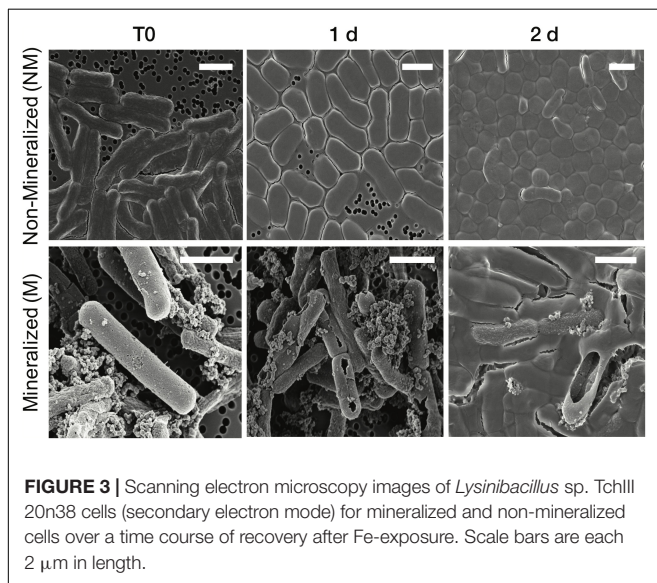
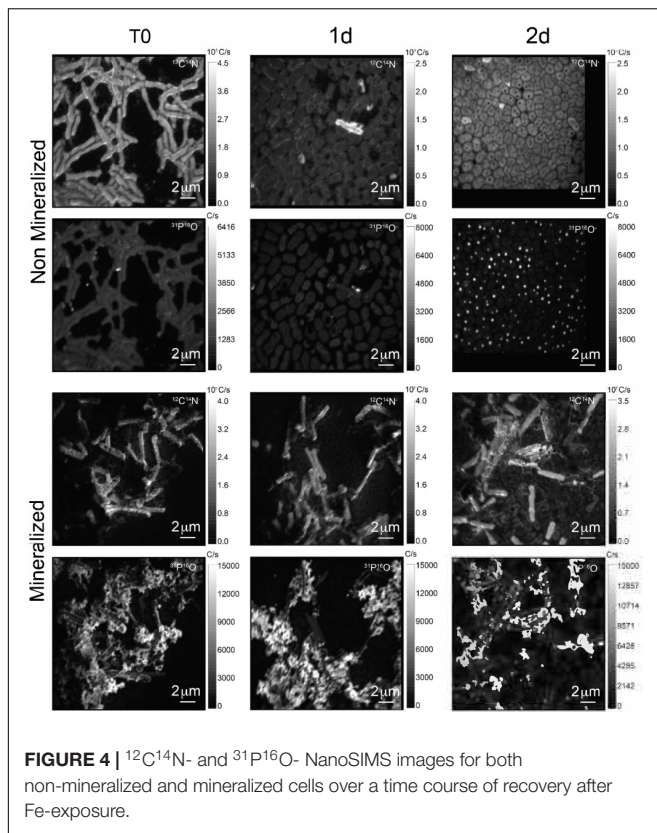


**FIGURE 3** | Scanning electron microscopy images of *Lysinibacillus* sp. TchlII 20n38 cells (secondary electron mode) for mineralized and non-mineralized cells over a time course of recovery after Fe-exposure. Scale bars are each 2  $\mu\text{m}$  in length.

is an effective marker, as S-layer proteins are one of the most abundant cellular proteins, and roughly 20% of total protein synthesis can be dedicated to their production (Sleytr et al., 2007). The  $^{15}\text{N}$  incorporation over time was determined using  $^{12}\text{C}^{15}\text{N}/(^{12}\text{C}^{15}\text{N}+^{12}\text{C}^{14}\text{N})$  and statistical analyses of the  $^{15}\text{N}/(^{14}\text{N}+^{15}\text{N})$  were then performed (see example of sample M\_T0\_rep2 in Figure 5 and Supplementary Figure S6). In order to account for differences in cell morphology over time and

between mineralized and non-mineralized samples, statistical analyses were performed using all pixels above the established threshold from each image. At least three processed  $^{15}\text{N}/(^{14}\text{N}+^{15}\text{N})$  images were analyzed per sample time point for samples incubated in medium containing  $^{15}\text{N}$  (two images each for natural abundance controls), with 10 to <60 cells per image depending on the physiological state of the cells over the time course. Subpopulations of pixels were identified for each sample according to the distribution of processed  $^{15}\text{N}/(^{14}\text{N}+^{15}\text{N})$  ratio (see Figure 5). Figure 5 shows that at the start of the time course (T0), the mineralized cells had  $^{15}\text{N}/(^{14}\text{N}+^{15}\text{N})$  ratios below 0.5 (panel A), with most cells having a ratio near 0.3 (panel B). Pixel subpopulations clustered around cells (panel C), with most mineralized cells and abiotic mineralization retaining a small amount of  $^{15}\text{N}$  (panel D) during the brief exposure prior to washing the cells in the first few minutes of the experiment.

Clustering of the NanoSIMS images according to their distribution of processed  $^{15}\text{N}/(^{14}\text{N}+^{15}\text{N})$  ratio showed that the samples tended to cluster over the experimental time course into three different groups; “natural abundance” ( $^{14}\text{N}$ ) T0 controls, low  $^{15}\text{N}$  incorporation (NM\_T0, M\_T0, M\_1d), and significant  $^{15}\text{N}$  incorporation (NM\_1d, NM\_2d, M\_2d) (see Figure 6). The fact that controls for the natural abundance (NM\_no incubation, M\_no incubation) grouped separately from the T0 samples shows that even brief exposure to the  $^{15}\text{N}$ -labeled medium during cell resuspension had an effect on the isotopic composition of the cells. The T0 samples were therefore used as the baseline of comparison for all later



time-points. The two remaining groups were composed of cells cultivated in  $^{15}\text{N}$ -labeled medium, grouped by whether or not cell division had restarted. Low  $^{15}\text{N}$ -incorporation samples (M\_T0, NM\_T0, M\_1d) corresponded to cells not yet showing evidence of cell division, whereas samples with significant  $^{15}\text{N}$  incorporation (NM\_1d, NM\_2d, M\_2d) showed clear evidence of active cell division when observed by SEM (see **Figure 3**) and measurements of optical density (see **Supplementary Figure S3**).

Variations between replicate images were minimal for all samples with the exception of both mineralized and non-mineralized 2 days samples, as seen in the heat map representation. The weighted distribution of subpopulations remained low for all samples prior to restart of cell division (see **Figure 6** and **Supplementary Figure S6**, samples M\_T0, M\_1d, NM\_T0). The increase in pixel subpopulations for samples showing signs of recovery and cell division (samples NM\_1d, NM\_2d, M\_2d) reflects the heterogeneity of cell recovery. Heterogeneity in  $^{15}\text{N}$  incorporation was highest for cells immediately after S-layer shedding (M\_2d samples), which is likely a reflection of natural variations in the capacity of *Lysinibacillus* sp. TchIII 20n38 cells to respond to stress.

## S-Layers Are Regenerated Within 2 Days of Fe-Mineral Encrustation

Some cell-free mineralized S-layer shells were observed by SEM immediately after 16 h exposure to the Fe-rich solution (see

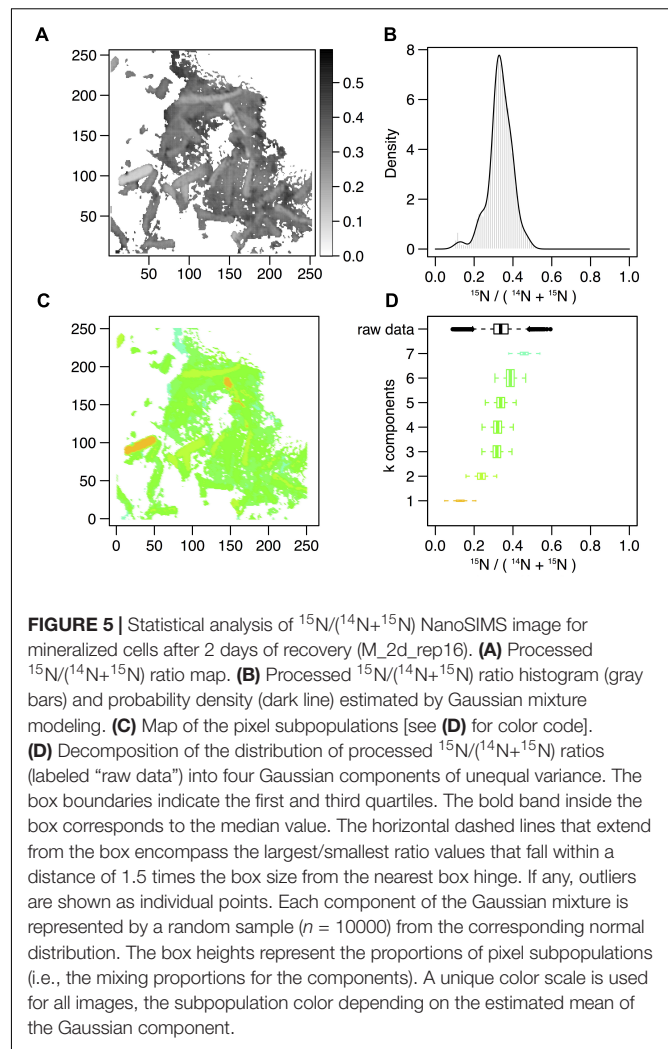


**Figure 3**). However, the morphology of the cells remained generally unchanged through 1 day of incubation in the defined medium. At 2 days of incubation in this medium, SEM observations clearly show a majority of non-mineralized cells alongside the remaining, cell-free, mineralized S-layer shells. Analyses of  $^{15}\text{N}$  uptake using NanoSIMS confirmed this timing, showing no significant  $^{15}\text{N}$  incorporation for mineralized samples prior to 2 days of recovery in labeled medium, compared to T0 control aliquots that were removed immediately after resuspension of cells in the labeled medium (see **Figure 6**). The S-layers of mineralized samples remained at a relatively steady  $^{15}\text{N}/(^{14}\text{N} + ^{15}\text{N})$  ratio (see green regions in **Supplementary Figure S6**, mineralized samples) compared to the emerging cells, showing that mineralized S-layers did not incorporate  $^{15}\text{N}$  during the cell division processes giving rise to the emerging cells. This is coherent with S-layer shedding and complete regeneration. S-layer presence before and after mineralization and shedding was confirmed by SDS-PAGE and mass spectrometry (see **Supplementary Figures S4, S5**).

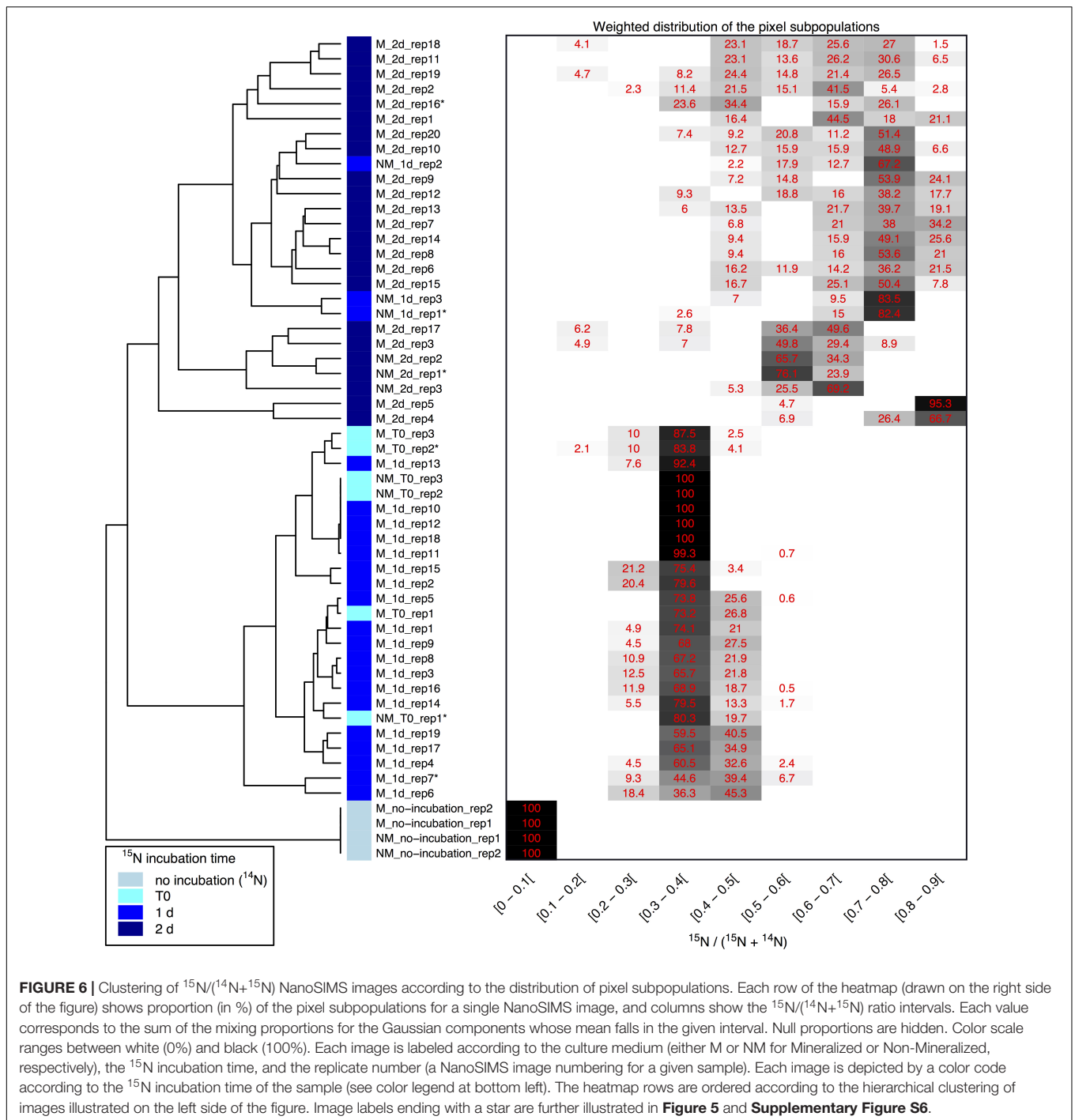


**FIGURE 6 |** Clustering of <sup>15</sup>N/(<sup>14</sup>N+<sup>15</sup>N) NanoSIMS images according to the distribution of pixel subpopulations. Each row of the heatmap (drawn on the right side of the figure) shows proportion (in %) of the pixel subpopulations for a single NanoSIMS image, and columns show the <sup>15</sup>N/(<sup>14</sup>N+<sup>15</sup>N) ratio intervals. Each value corresponds to the sum of the mixing proportions for the Gaussian components whose mean falls in the given interval. Null proportions are hidden. Color scale ranges between white (0%) and black (100%). Each image is labeled according to the culture medium (either M or NM for Mineralized or Non-Mineralized, respectively), the <sup>15</sup>N incubation time, and the replicate number (a NanoSIMS image numbering for a given sample). Each image is depicted by a color code according to the <sup>15</sup>N incubation time of the sample (see color legend at bottom left). The heatmap rows are ordered according to the hierarchical clustering of images illustrated on the left side of the figure. Image labels ending with a star are further illustrated in **Figure 5** and **Supplementary Figure S6**.

## DISCUSSION

### *Lysinibacillus* sp. TchIII 20n38 Is Highly Adapted for Survival Under Stress Conditions

The bacterial isolate used in this study, *Lysinibacillus* sp. TchIII 20n38, is a metallotolerant gram-positive bacterium, possessing a cell envelope composed of the plasma membrane

surrounded by a thick layer of peptidoglycan capped by an S-layer forming an ordered structure at the cell surface. This flexible cage-like structure is in direct contact with the surrounding environment, and thus provides the primary protective element against potentially toxic environmental concentrations of heavy metals or radionuclides. Such interactions between *Lysinibacillus* sp. cells and metals can lead to cell surface mineralization, biosorption, or intracellular bioaccumulation, depending on the depending on the types of metals present and physicochemical

parameters such as pH (data not shown). Here, we show that *Lysinibacillus* sp. TchIII 20n38 has many adaptive mechanisms to the stresses induced by nutrient limitation and/or the presence of iron, as might be expected for a bacterium isolated from a radioactive waste disposal site. These included the accumulation and enlargement of intracellular polyphosphate granules and sporulation under phosphate-limiting conditions, cell size reduction, and morphology alterations from rod-shaped to ovoid cells after metal stress, as well as reductions in biofilm after exposure to either iron or acidic pH and augmentation in biofilm after a return to neutral pH in the absence of additional iron input. Polyphosphate accumulation is a common mechanism used by bacteria, including *Lysinibacillus sphaericus*, in response to nutrient stress (depletion of amino acids), and prior to sporulation (Tocheva et al., 2013; Shi et al., 2015).

### S-Layer Shedding Mechanism in *Lysinibacillus* as a Response to Metal Stress

S-Layers from a variety of prokaryotes are known to induce mineral formation. The S-layers of cyanobacteria are able to nucleate selenite and strontium (Schultze-Lam and Beveridge, 1994), while the S-layers of thermophilic archaea can form amorphous Fe-phosphate minerals in the quasi-periplasmic space between the S-layer and the underlying lipid membrane (Kish et al., 2016). Diverse *Lysinibacillus* sp. have been observed to precipitate minerals on their cell surfaces, including U-phosphates (Merroun et al., 2005; Mondani et al., 2011) and calcium carbonate (Kaur and Mukherjee, 2013). Here, we show that *Lysinibacillus* sp. TchIII 20n38 cells become encrusted with Fe-minerals after exposure to high concentrations of iron under mildly acidic conditions. Mineral precipitation by the cell surfaces, including S-layers, prevent damages to cells including oxidative stress, enzyme deactivation, protein denaturation, and membrane disruption (Lemire et al., 2013). Iron precipitation nucleated by the S-layer proteins prevents an overproduction of free radicals in the cytosol due to Fenton chemistry.

While mineral formation on S-layers is known, the mechanisms for removing such barriers to exchange with the surrounding environment are not as well-understood. Mechanisms identified to date have described partial removal of cell envelope components after metal interactions, particularly membrane vesicle formation (McBroom and Kuehn, 2007; Shao et al., 2014; Kish et al., 2016). Partial shedding of S-layer fragments has also been observed, both for mineralized cyanobacterial S-layers (Schultze-Lam et al., 1992; Schultze-Lam and Beveridge, 1994) and non-mineralized S-layers for stationary phase bacteria likely as part of cell wall turnover (Luckevich and Beveridge, 1989). During the course of normal cell growth in the closely related *Lysinibacillus sphaericus*, bands of S-layer monomer insertion form on cell surfaces, and in the course of cell division new S-layer monomers are only inserted at the newly-formed the poles (Howard et al., 1982).

Here, we show that *Lysinibacillus* sp. cells were able to recover normal growth after mineral encrustation through a shedding of

mineralized S-layers, followed by S-layer regeneration. To our knowledge, this is the first report of complete S-layer shedding and regeneration. S-layer shedding required an additional 24h before cells returned to normal cell division compared to non-mineralized cells, as shown by the clustering of  $^{15}\text{N}$  uptake by 2 days mineralized cells with 1 day non-mineralized samples as measured by NanoSIMS over a time course after exposure to iron. Uptake of  $^{15}\text{N}$  also illustrated that despite extensive mineralization, cells retained active metabolism. The continued presence of shed, mineralized S-layers composed of  $^{14}\text{N}$ -based proteins alongside cells bearing newly regenerated  $^{15}\text{N}$ -bearing S-layers resulted in the heterogeneity in  $^{15}\text{N}$ -incorporation for the M\_2d samples (see **Figure 6**). S-layer shedding activity was limited to cells in mid-exponential growth phase, providing an advantage over cells in stationary growth phase in Fe-rich conditions.

### Importance of S-Layer Regeneration in Metal Stress

Now that the mechanism for S-layer shedding has been established for *Lysinibacillus* sp. TchIII 20n38, future work should explore the range of different metals that can be mineralized by S-layers, both in this bacterium and other S-layer bearing bacteria including both Gram-negative and Gram-positive species. The high diversity of S-layer bearing bacterial species suggests that this mechanism could be widely used. Shedding of mineralized S-layers is less likely in the Archaea, given that for many species the S-layer is the sole component of their cell wall. Indeed, our previous work in the archaeon *Sulfolobus acidocaldarius* demonstrated that S-layer shedding was not observed; mineralized S-layers were rather partially sloughed off by the formation of membrane vesicles prior to cell encrustation (Kish et al., 2016).

The S-layer shedding and regeneration shown here after mineral encrustation may also inform new directions for S-layer use in *in situ* bioremediation. Current biotechnology applications of S-layers focus on *in vitro* applications such as the use of recombinant S-layer proteins with enhanced metal binding capacity (Pollmann and Matys, 2007), or as templates to nucleate the fabrication of metal nanoparticle biocatalysts (Creamer et al., 2007), or as bio-filters for bioremediation technologies (Pollmann et al., 2006). S-layer regeneration after mineralization may aid the development of new metal remediation strategies using metallotolerant soil bacteria native to soils contaminated by metals and radionuclides to reduce the bioavailability of toxic metals through mineralization.

### AUTHOR CONTRIBUTIONS

AK and LR contributed to conception and design of the study. AC performed the experiments and wrote sections of the manuscript. LR performed the NanoSIMS measurements. CL and SZ performed the mass spectrometry analyses. ED performed the statistical analysis of NanoSIMS data. AK wrote the first draft of the manuscript.



All authors contributed to manuscript revision, read and approved the submitted version.

## FUNDING

This work was supported by the French National Program EC2CO-MicrobiEn, project “SkinDEEP,” awarded to AK. The National NanoSIMS facility at the MNHN was established by funds from the CNRS, Région Ile de France, Ministère Délégué à l’Enseignement Supérieur et à la Recherche, and the MNHN. The SEM facility of the Institut de Minéralogie, Physique des Matériaux et Cosmochimie is supported by Région Ile de France grant SESAME 2006 NoI-07-593/R, INSU-CNRS, INP-CNRS, Sorbonne Universités, and by the French National Research Agency (ANR) (Grant No. ANR-07-BLAN-0124-01).

## REFERENCES

- Ahmed, I., Yokota, A., Yamazoe, A., and Fujiwara, T. (2007). Proposal of *Lysinibacillus boronitoleras* gen. nov. sp. nov., and transfer of *Bacillus fusiformis* to *Lysinibacillus fusiformis* comb. nov. and *Bacillus sphaericus* to *Lysinibacillus sphaericus* comb. nov. *Int. J. Syst. Evol. Microbiol.* 57, 1117–1125. doi:10.1099/ijs.0.63867-0
- Benaglia, T., Chauveau, D., Hunter, D. R., and Young, D. (2009). mixtools: an RPackage for analyzing finite mixture models. *J. Stat. Softw.* 32, 1–29. doi: 10.18637/jss.v032.i06
- Chapon, V., Piette, L., Vesvres, M.-H., Coppin, F., Marrec, C. L., Christen, R., et al. (2012). Microbial diversity in contaminated soils along the T22 trench of the Chernobyl experimental platform. *Appl. Geochem.* 27, 1375–1383. doi: 10.1016/j.apgeochem.2011.08.011
- Creamer, N. J., Mikheenko, I. P., Yong, P., Deplanche, K., Sanyahumbi, D., Wood, J., et al. (2007). Novel supported Pd hydrogenation bionanocatalyst for hybrid homogeneous/heterogeneous catalysis. *Catal. Today* 128, 80–87. doi: 10.1016/j.cattod.2007.04.014
- Howard, L. V., Dalton, D. D., and McCoubrey, W. K. (1982). Expansion of the tetragonally arrayed cell wall protein layer during growth of *Bacillus sphaericus*. *J. Bacteriol.* 149, 748–757.
- Kaur, D. N., and Mukherjee, A. (2013). Biomineralization of calcium carbonate polymorphs by the bacterial strains isolated from calcareous sites. *J. Microbiol. Biotechnol.* 23, 707–714. doi: 10.4014/jmb.1212.11087
- Kish, A., Miot, J., Lombard, C., Guigner, J.-M., Bernard, S., Zirah, S., et al. (2016). Preservation of archaeal surface layer structure during mineralization. *Sci. Rep.* 6:26152. doi: 10.1038/srep26152
- Konhauser, K. O., Schultze-Lam, S., Ferris, F. G., Fyfe, W. S., Longstaffe, F. J., and Beveridge, T. J. (1994). Mineral precipitation by epilithic biofilms in the Speed river, Ontario, Canada. *Appl. Environ. Microbiol.* 60, 549–553.
- Lemire, J. A., Harrison, J. J., and Turner, R. J. (2013). Antimicrobial activity of metals: mechanisms, molecular targets and applications. *Nat. Rev. Microbiol.* 11, 371–384. doi: 10.1038/nrmicro3028
- Luckevich, M. D., and Beveridge, T. J. (1989). Characterization of a dynamic S layer on *Bacillus thuringiensis*. *J. Bacteriol.* 171, 6656–6667. doi: 10.1128/jb.171.12.6656-6667.1989
- McBroom, A. J., and Kuehn, M. J. (2007). Release of outer membrane vesicles by Gram-negative bacteria is a novel envelope stress response. *Mol. Microbiol.* 63, 545–558. doi: 10.1111/j.1365-2958.2006.05522.x
- Merroun, M. L., Raff, J., Rossberg, A., Hennig, C., Reich, T., and Selenska-Pobell, S. (2005). Complexation of uranium by cells and S-layer sheets of *Bacillus sphaericus* JG-A12. *Appl. Environ. Microbiol.* 71, 5532–5543. doi: 10.1128/AEM.71.9.5532-5543.2005

## ACKNOWLEDGMENTS

We gratefully acknowledge Virginie Chapon for giving us the strain used in this study, along with helpful discussions. We thank Adriana Gonzalez-Cano and Rémi Duhamel for assistance with NanoSIMS analyses, and Imène Esteve of the SEM facility of the Institut de Minéralogie, Physique des Matériaux et Cosmochimie for assistance with imaging, which was greatly appreciated. We also wish to thank Jennyfer Miot for productive discussions.

## SUPPLEMENTARY MATERIAL

The Supplementary Material for this article can be found online at: <https://www.frontiersin.org/articles/10.3389/fmicb.2018.03210/full#supplementary-material>

- Miot, J., Remusat, L., Duprat, E., Gonzalez, A., Pont, S., and Poinso, M. (2015). Fe biomineralization mirrors individual metabolic activity in a nitrate-dependent Fe(II)-oxidizer. *Front. Microbiol.* 6:879. doi: 10.3389/fmicb.2015.00879
- Mondani, L., Benzerara, K., Carrière, M., Christen, R., Mamindy-Pajany, Y., Février, L., et al. (2011). Influence of uranium on bacterial communities: a comparison of natural uranium-rich soils with controls. *PLoS One* 6:e25771. doi:10.1371/journal.pone.0025771
- Phoenix, V. R., Adams, D. G., and Konhauser, K. O. (2000). Cyanobacterial viability during hydrothermal biomineralisation. *Chem. Geol.* 169, 329–338. doi: 10.1016/S0009-2541(00)00212-6
- Pollmann, K., and Matys, S. (2007). Construction of an S-layer protein exhibiting modified self-assembling properties and enhanced metal binding capacities. *Appl. Microbiol. Biotechnol.* 75, 1079–1085. doi: 10.1007/s00253-007-0937-5
- Pollmann, K., Raff, J., Merroun, M., Fahmy, K., and Selenska-Pobell, S. (2006). Metal binding by bacteria from uranium mining waste piles and its technological applications. *Biotechnol. Adv.* 24, 58–68. doi: 10.1016/j.biotechadv.2005.06.002
- R Core Team (2015). *R: A Language and Environment for Statistical Computing*. Vienna: R Foundation for Statistical Computing.
- Rodriguez-Freire, L., Avsarala, S., Ali, A.-M. S., Agnew, D., Hoover, J. H., Artyushkova, K., et al. (2016). Post gold king mine spill investigation of metal stability in water and sediments of the animas river watershed. *Environ. Sci. Technol.* 50, 11539–11548. doi: 10.1021/acs.est.6b03092
- Schultze-Lam, S., and Beveridge, T. J. (1994). Nucleation of celestite and strontianite on a cyanobacterial s-layer. *Appl. Environ. Microbiol.* 60, 447–453.
- Schultze-Lam, S., Harauz, G., and Beveridge, T. J. (1992). Participation of a cyanobacterial S layer in fine-grain mineral formation. *J. Bacteriol.* 174, 7971–7981. doi: 10.1128/jb.174.24.7971-7981.1992
- Scrucca, L., Fop, M., Murphy, T. B., and Raftery, A. E. (2016). mclust 5: clustering, classification and density estimation using gaussian finite mixture models. *R J.* 8, 289–317.
- Shao, P. P., Comolli, L. R., and Bernier-Latmani, R. (2014). Membrane vesicles as a novel strategy for shedding encrusted cell surfaces. *Minerals* 4, 74–88. doi: 10.3390/min4010074
- Shi, T., Ge, Y., Zhao, N., Hu, X., and Yuan, Z. (2015). Polyphosphate kinase of *Lysinibacillus sphaericus* and its effects on accumulation of polyphosphate and bacterial growth. *Microbiol. Res.* 172, 41–47. doi: 10.1016/j.micres.2014.12.002
- Sleytr, U. B., Egelseer, E. M., Ilk, N., Pum, D., and Schuster, B. (2007). S-Layers as a basic building block in a molecular construction kit. *FEBS J.* 274, 323–334. doi: 10.1111/j.1742-4658.2006.05606.x
- Sleytr, U. B., Schuster, B., Egelseer, E. M., and Pum, D. (2014). S-layers: principles and applications. *FEMS Microbiol. Rev.* 38, 823–864. doi: 10.1111/1574-6976.12063

- Sleytr, U. B., Schuster, B., Egelseer, E. M., Pum, D., Horejs, C. M., Tscheliessnig, R., et al. (2011). Nanobiotechnology with S-layer proteins as building blocks. *Prog. Mol. Biol. Transl. Sci.* 103, 277–352. doi: 10.1016/B978-0-12-415906-8.00003-0
- Thomen, A., Robert, F., and Remusat, L. (2014). Determination of the nitrogen abundance in organic materials by NanoSIMS quantitative imaging. *J. Anal. At. Spectrom.* 29, 512–519. doi: 10.1039/c3ja50313e
- Tocheva, E. I., Dekas, A. E., McGlynn, S. E., Morris, D., Orphan, V. J., and Jensen, G. J. (2013). Polyphosphate storage during sporulation in the gram-negative bacterium *Acetonema longum*. *J. Bacteriol.* 195, 3940–3946. doi: 10.1128/JB.00712-13

**Conflict of Interest Statement:** The authors declare that the research was conducted in the absence of any commercial or financial relationships that could be construed as a potential conflict of interest.

Copyright © 2019 Chandramohan, Duprat, Remusat, Zirah, Lombard and Kish. This is an open-access article distributed under the terms of the Creative Commons Attribution License (CC BY). The use, distribution or reproduction in other forums is permitted, provided the original author(s) and the copyright owner(s) are credited and that the original publication in this journal is cited, in accordance with accepted academic practice. No use, distribution or reproduction is permitted which does not comply with these terms.